Labeling and Probing the Silica Surface Using Mechanochemistry and ^{17}O NMR Spectroscopy**

Chia-Hsin Chen,*[a] Frederic Mentink-Vigier,[b] Julien Trébosc,[c] Ieva Goldberga,[a] Philippe Gaveau,[a] Emilie Thomassot,[d] Dinu Iuga,[e] Mark E. Smith,[f] Kuizhi Chen,[b] Zhehong Gan,[b] Nicolas Fabregue,[a] Thomas-Xavier Métro,[g] Bruno Alonso,*[a] and Danielle Laurencin*[a]

Abstract: In recent years, there has been increasing interest in developing cost-efficient, fast, and user-friendly ^{17}O enrichment protocols to help to understand the structure and reactivity of materials by using ^{17}O NMR spectroscopy. Here, we show for the first time how ball milling (BM) can be used to selectively and efficiently enrich the surface of fumed silica, which is widely used at industrial scale. Short milling times (up to 15 min) allowed modulation of the enrichment level (up to ca. 5%) without significantly changing the nature of the material. High-precision ^{17}O compositions were measured at different milling times by using large-geometry secondary-ion mass spectrometry (LG-SIMS). High-resolution ^{17}O NMR analyses (including at 35.2 T) allowed clear identification of the signals from siloxane (Si–O–Si) and silanols (Si–OH), while DNP analyses, performed by using direct ^{17}O polarization and indirect $^{17}O\{^1H\}$ CP excitation, agreed with selective labeling of the surface. Information on the distribution of Si–OH environments at the surface was obtained from 2D ^1H–^{17}O D-HMQC correlations. Finally, the surface-labeled silica was reacted with titania and using ^{17}O DNP, their common interface was probed and Si–O–Ti bonds identified.

Introduction

Silica, one of the most studied oxides, is used in a very wide range of applications on the industrial scale.[1] It can for example serve as a reagent for the production of cement and glass, as a filler in polymers and pastes, as an additive in the cosmetics and pharmaceutical industries, or as support for metallic and organometallic catalysts. It can be used either in crystalline or amorphous form, as dense or porous solids, and can be associated with very different materials, leading to mixed oxide ceramics and glasses or organic-inorganic hybrids and composites. In applications of high surface area silica phases (for porous and particulate materials), the surface chemistry of silica plays an important role during the formation of interfaces with organic or inorganic components. This surface reactivity relies notably on the quantity and structural environments of surface hydroxyl groups. Many research groups have thus focused on developing experimental and computational techniques enabling understanding in detail the structure and reactivity of silica surfaces, in particular for amorphous silica which can display a wide diversity of siloxane (Si–O–Si) and silanol (Si–OH) bonding environments.[2–11] The surface of amorphous silica

[a] Dr. C.-H. Chen, Dr. I. Goldberga, Dr. P. Gaveau, N. Fabregue, Dr. B. Alonso, Dr. D. Laurencin
ICGM, Univ Montpellier, CNRS, ENSCMMontpellier (France)
E-mail: chia-hsin.chen@umontpellier.fr
bruno.alonso@enscm.fr
danielle.laurencin@umontpellier.fr

[b] Dr. F. Mentink-Vigier, Dr. K. Chen, Dr. Z. Gan
National High Magnetic Field Laboratory (NHMFL)
Florida State University
Tallahassee, FL (USA)

[c] Dr. J. Trébosc
Univ. Lille, CNRS, INRAE, Centrale Lille, Univ. Artois
FR 2638 – IMEC – Institut Michel-Eugène Chevreul
59000 Lille (France)

[d] Dr. E. Thomassot
Université de Lorraine
CRPG, CNRS UMR 7358
Vandœuvre-lès-Nancy (France)

[e] Dr. D. Iuga
Department of Physics
University of Warwick
CV4 7AL Coventry (UK)

[f] Prof. M. E. Smith
Vice-Chancellor's Office and Department of Chemistry
Highfield Campus, University of Southampton
SO17 1BJ Southampton (UK)

[g] Dr. T.-X. Métro
IBMM, Univ Montpellier, CNRS, ENSCM
Montpellier (France)

[**] A previous version of this manuscript has been deposited on a preprint server (https://doi.org/10.26434/chemrxiv.14414027.v1).

Supporting information for this article is available on the WWW under https://doi.org/10.1002/chem.202101421

phases varies depending on how the material is produced and stored. For example, it has been reported that an untreated fumed silica referred to as Cab–O–Sil consists of both hydrogen-bonded silanols and isolated silanols on its surface, while an untreated silica gel phase only has hydrogen-bonded silanols on its surface.[7]

Solid-state nuclear magnetic resonance (NMR) is a powerful tool for characterizing materials on an atomic scale, which can provide information about bonding schemes and structures. In the case of silica, ^{29}Si NMR analyses can inform on the condensation degree of the silica phase (siloxane vs. silanol content).[12] Moreover, ^{1}H NMR analyses have been used early on, for example, to investigate the hydration and dehydration of silica phases, and/or to identify isolated silanols and hydrogen-bonded silanols on the silica surface.[3,7,11] The ^{1}H chemical shifts of silanols are sensitive to hydrogen-bonding and have been used to estimate the hydration level of silica surfaces.[7,13] However, because the ^{1}H signals of water, hydrogen-bonded silanols, and isolated silanols can overlap significantly, their detailed characterization remains difficult. Despite their interesting features, ^{29}Si and ^{1}H NMR analyses cannot provide full information on the diversity of oxygen sites arising from surface siloxanes and silanols, nor on the diversity of hydrogen-bond networks they can be engaged in.

Oxygen-17 NMR naturally appears as a valuable technique for underpinning a better understanding of the different surface oxygen bonding environments, as the chemical shifts and quadrupolar parameters of this isotope are very sensitive to small structural changes in the vicinity of the oxygen.[14–17] As a matter of fact, previous experimental and computational studies have suggested that ^{17}O NMR parameters can reflect the diversity of siloxane and silanol sites at the surface of silica.[2,4,5,18,19] Moreover, it was also found that the surface of silica grafted by organometallic fragments could be probed by ^{17}O NMR (including dynamic nuclear polarization – DNP – enhancement in some cases), which revealed Si–OH, Si–O–Si, and Si–O–M (M=Zr, Ta, W) environments, and showed how ^{17}O chemical shifts and quadrupolar parameters are sensitive to surface modifications.[18,20,21] However, despite these highly promising results, ^{17}O NMR is still not routinely used for the characterization of the surface of silica phases, due to its very low natural abundance (only 0.037%), which implies that ^{17}O-enriched phases need to be prepared to perform high-resolution NMR analyses.

Due to the importance of silica as a material, several labeling routes have been proposed early on for the enrichment of this phase, mainly using ^{17}O-enriched H_2O as a precursor.[22–26] Most frequently, the ^{17}O enrichment of bulk silica is carried out by hydrolysis of silicon tetrachloride ($SiCl_4$) with $H_2{}^{17}O$ in diethyl ether at low temperature (e.g. 0 °C). The dried product can then be heated up at 200 °C under vacuum to form an amorphous silica phase or can be subsequently heated up to 1800 °C under an inert atmosphere to transform to glass.[24–26] An alternative method consists of using $H_2{}^{17}O$ in the hydrolysis of a silicon alkoxide, in a sol-gel process which can be used to prepare not only pure ^{17}O enriched silica (when using for instance tetraethyl orthosilicate (TEOS)), but also ^{17}O enriched mixed oxides or hybrid materials (e.g. by mixing TEOS with metal alkoxide precursors).[27–30] Here, it is often necessary to optimize the hydrolysis and condensation steps, as well as the final heat-treatment step to eliminate organic fragments, in order to obtain pure products.[31] These two methods have the advantage of homogenously enriching oxygen sites in the bulk sample during synthesis. It has also been shown that is possible to selectively post-enrich the surface of silica in ^{17}O. For example, Merle et al. exposed an amorphous silica phase (Aerosil 200) which had been pre-dried at 1000 °C under high vacuum to an excess of $H_2{}^{17}O$ for 8 h, after which they performed a heat treatment under vacuum and obtained a surface-enriched fumed silica.[18] A similar method was also successfully applied to enrich the surface of mesoporous silica phases (SBA and MCM-41).[21,32]

Nevertheless, whether for bulk or surface, the ^{17}O enrichment of silica is still not widely used. This can be partly explained by the synthetic challenges associated with the protocols described so far. The experimental conditions used in these protocols for performing the labeling are time-consuming and/or experimentally demanding, by requiring to perform reactions in an inert atmosphere or at very high temperatures. Therefore, these protocols are rarely optimized due to experimental constraints, and unattractive for routine analyses by ^{17}O NMR.

In a recent study, we showed that various oxides including silica can be labeled in ^{17}O using a user-friendly and cost-efficient ^{17}O enrichment protocol involving mechanochemistry.[33] More specifically, it had been demonstrated that using the liquid-assisted grinding (LAG) approach, fumed silica (Aerosil) can be efficiently enriched in 60 minutes while working under ambient temperature and pressure, which is a clear advantage compared to previous protocols.[33] However, these milling conditions were found to induce some changes in composition and texture of the silica phase, such as a decrease in the specific surface area (by a factor of ≈3), and the presence of impurities coming from the milling jar (e.g. Fe and Cr). Such paramagnetic elements can be problematic if the enriched silica phase is to be used as a precursor for the synthesis of functional materials, and also because they may prevent some high-resolution solid-state NMR experiments to be performed, due to shortened NMR relaxation times. Moreover, the possibility to selectively enrich the surface of the silica precursor had not been explored.

In this manuscript, we investigate for the first time the easy preparation of a ^{17}O-surface enriched silica phase under mild conditions using LAG. The labeling of Aerosil 200, a fumed silica phase composed of aggregated nanoparticles, was performed using an optimized ball milling protocol. First, a detailed characterization of enriched phases isolated after two milling times is presented using TEM, EDXS, N_2 adsorption volumetry, and IR spectroscopy, showing that the milling process leads to fewer changes in texture and impurities than previously, and providing a better understanding of the milling process. Then, the results from the ^{17}O enrichment levels measured by LG-SIMS and from high-resolution ^{17}O NMR (including at ultra-high magnetic fields) and DNP analyses are discussed, from which it

can be concluded that it is the surface of the particles which is enriched. Detailed insights into the variety of local oxygen environments and reactivity of the labeled surface of silica are shown, on the basis of complementary ^{1}H–^{17}O correlation experiments (which shed light on the H-bond network). Lastly, studies of the reactivity of this oxide by using the formation of mixed titania-silica phases were performed, which opens up many perspectives for future uses of such surface-labeled phases for complex materials analyses.

Results and Discussion

^{17}O Enrichment of silica under mild conditions by using LAG

A fumed silica made of aggregated nanoparticles (Aerosil 200, average diameter of particles ≈12 nm, according to the supplier) was milled with stoichiometric amounts of ≈90% $H_2{}^{17}O$ for 5 and 15 minutes in a vertical mixer mill using a hardened stainless steel jar and milling balls, and a set milling frequency of 25 Hz (Figure 1a). In ball milling, particles are subjected to impact and shear forces, with the movement of the milling balls in the jars having a direct impact on the nature of the surfaces created. The milled Aerosil was thus character-

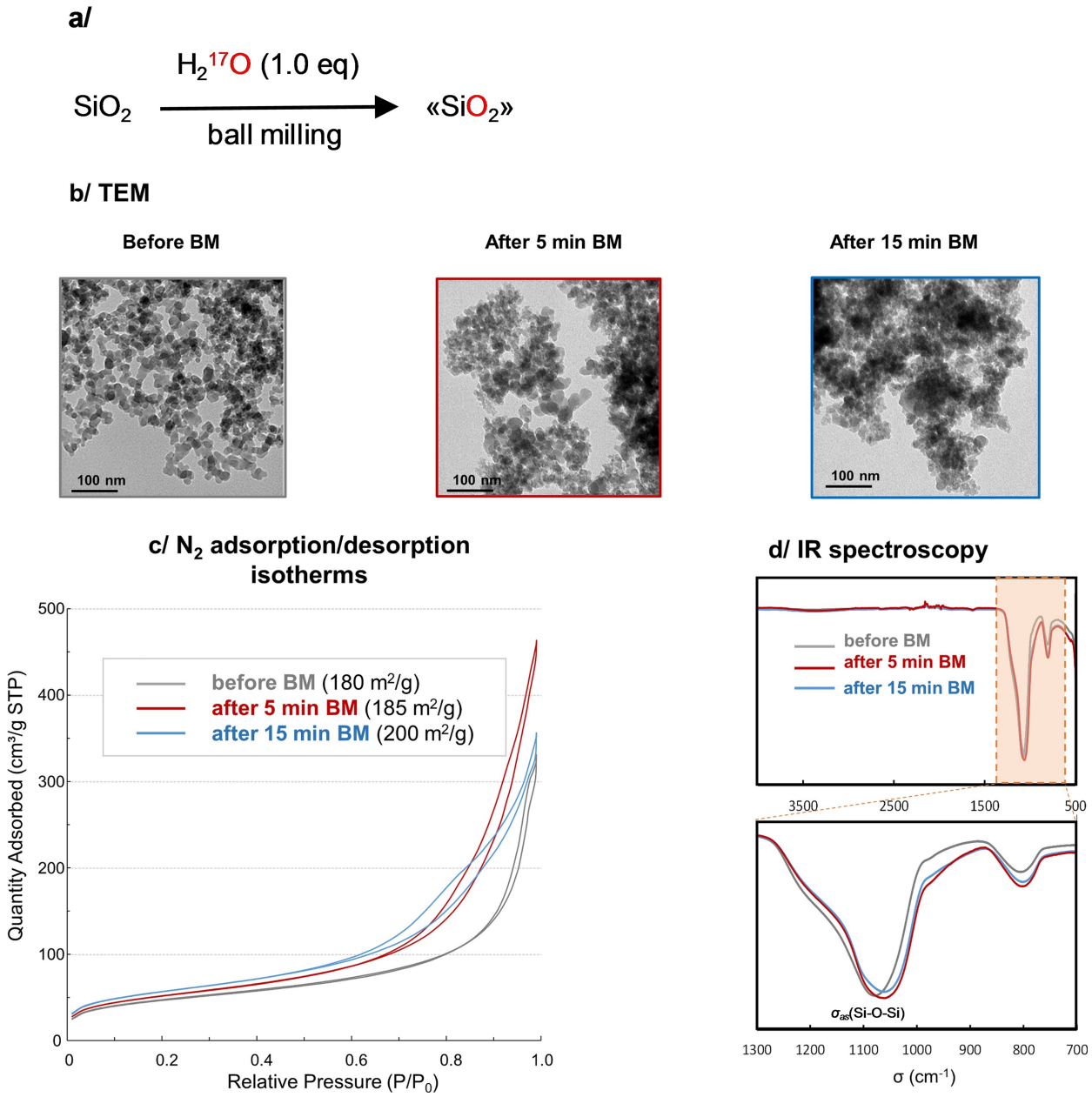

Figure 1. ^{17}O labeling scheme and characterizations of the silica precursor (Aerosil), BM_{5min}–SiO_2, and BM_{15min}–SiO_2: (a) General ^{17}O labeling scheme of silica using LAG, (b) TEM images, (c) N_2 adsorption and desorption isotherms (77 K), and (d) IR spectra.

ized by a wide range of techniques to identify possible changes in texture and structure.

No new phase was observed by PXRD after 15 minutes of milling (Figure S1b). More importantly, no Fe or Cr impurities were detected by EDXS, even after 15 minutes of milling (Figure S1c). In TEM, the Aerosil precursor showed aggregations of nanoparticles with evenly distributed particle sizes (diameter ≈10–20 nm). After 5 and 15 minutes of milling, the particles were more aggregated suggesting a decrease in meso- and macro-porosity. However, individual particles could still be identified, yet with a wider size distribution (Figure 1b). According to TEM, BM_{5min}–SiO_2 appeared to be an intermediate stage between the Aerosil precursor and BM_{15min}–SiO_2 (Figure 1b).

Information on the external surface of the aggregated silica nanoparticles could be obtained by the BET specific surface area S_{BET} (Figure 1c), which was estimated from N_2 adsorption/desorption isotherms. S_{BET} values of Aerosil precursor, BM_{5min}–SiO_2, and BM_{15min}–SiO_2 did not show significant variations (180, 185, and 200 m^2/g respectively). This result suggests that the overall surface/volume ratio for the aggregated silica nanoparticles, and thus in their mean particle size, is preserved after BM, in agreement with TEM observations. The more noticeable change in the N_2 adsorption/desorption experiments was in the shape of the N_2 isotherms. After ball milling, the hysteresis loop, related to the capillary condensation in mesopores, was more pronounced and shifted towards lower relative p/p_0 pressures. These changes can be explained by a modification in the pore size distribution (PSD), and the notable decrease in average pore sizes, corresponding to the reduction in the size of the voids between silica nanoparticles observed by TEM. Further analyses of PSD as a function of the milling time were performed, showing that most of the changes in pore geometry and PSD occur within the first 5 minutes (Figure S1d). It is worth noting here that the N_2 adsorption analyses were found to demonstrate the high reproducibility of the milling procedure, in yielding a given PSD.

Using infrared spectroscopy, a shift of ≈20 cm^{-1} to lower wavenumbers of the broad Si–O–Si asymmetric stretching band σ_{as}(Si–O–Si) was observed after 5 and 15 minutes of milling (Figure 1d). The possibility of this being due to an isotopic shift caused by siloxane labeling was examined by comparing additional samples made with $H_2{}^{16}O$ and $H_2{}^{18}O$ using the same LAG approach (Table S2). No significant shifts in siloxane frequency were observed between these differently labeled samples, indicating the change in σ_{as}(Si–O–Si) is not related to an isotopic shift. The variation of the σ_{as}(Si–O–Si) band towards lower wavenumbers may thus rather suggest slightly longer average Si–O bond lengths after ball milling,[34] indicating that changes in siloxane bonds are occurring during the milling. Additional ^{29}Si NMR experiments were carried out to further study this point, as detailed below. However, because IR spectroscopy analyses suggested that the enrichment was a priori limited, quantitative analyses were performed to determine the actual enrichment level of the milled silica.

Enrichment level and model of the surface labeling

Large-geometry secondary-ion mass spectrometry (LG-SIMS) was used to determine the absolute ^{17}O enrichment of milled silica. This technique allows the composition of the first few atomic layers to be analyzed.[35] For the synthetic conditions used in our LAG protocol (one equivalent $H_2{}^{17}O$ (90% ^{17}O) reacting with one equivalent SiO_2), the maximum absolute enrichment was expected to be ≈30% when considering a full isotopic scrambling between ^{17}O and ^{16}O sites upon milling. Here, the absolute ^{17}O enrichment was found to be ≈2.2 (±0.2) % after 5 minutes of milling. The $^{17}O/^{16}O$ isotopic ratio was found to further increase by a factor of ≈2.4 after 15 minutes of milling (see Supporting Information Table S1), leading to an estimated absolute enrichment of ≈5.3% for BM_{15min}–SiO_2. It is worth noting here that this overall increase in ^{17}O content was also observed in ^{17}O NMR, when recording the ^{17}O MAS NMR spectra of BM_{5min}–SiO_2 and BM_{15min}–SiO_2 samples using acquisition conditions allowing directly quantitative comparison of signal integrals (i.e. similar NMR acquisition parameters, including a small tip-angle, and similar masses of sample analyzed; see Supporting Information, Figure S2a).

Both ^{17}O-enrichment levels were found to be lower than ≈30%, suggesting the isotopic scrambling was not complete after 15 minutes of milling. Given that the enrichment level increases between 5 and 15 minutes, a higher enrichment level could potentially have been reached using longer milling times. Indeed, in our previous investigation on the enrichment of Aerosil by mechanochemistry (which had been performed under different milling conditions, in terms of mixer mill used, number of beads, and level of filling of the milling jar),[33] a nearly complete oxygen isotopic scrambling had been reached after ≈1 h of milling. However, we did not attempt using longer milling times in this work in order to label specifically the silica surface and to avoid a potential decrease in surface area and the possible contamination by impurities under such conditions.[33] It is worth noting that the enrichment level of milled silica obtained from SIMS might be slightly underestimated because SIMS is operated under ultrahigh vacuum (≈10^{-9} mbar), which could lead to the loss of some of the ^{17}O enriched OH groups of the surfaces (removed in the form of water). However, considering the full range of ^{17}O NMR characterizations of the samples described below, this would only lead to a moderate underestimation of the actual ^{17}O-labeling after BM.

A possible interpretation of the ^{17}O-enrichment values measured for the silica phases after 5 and 15 minutes of ball milling can be proposed, based on observation by TEM that aggregated nanoparticles were globally preserved after LAG and assuming that the enrichment proceeds from the surface towards the center of the particles, as suggested in our previous work for other oxides like titania.[33] We can then consider a simplified model of a fully ^{17}O-enriched shell and a core of non-enriched silica, and assume, as a first approximation, that the nanoparticles are well-defined spheres, and homogenous in size. Using this model, for a nanoparticle of ≈10 nm in diameter enriched in ^{17}O at ≈5%, it was found that this enrichment

would only correspond to a very thin shell of approximately 1 Å (Figure S3). Although this assumption of a fully enriched shell and a spherical nanoparticle geometry does not strictly correspond to the real state of the milled silica, nevertheless, it tends to indicate that only the outer surface of the silica nanoparticles, or the interface between aggregated particles, was enriched by LAG. This estimation of a very thin labeled surface layer confirms *a posteriori* the validity of the use of LG-SIMS for quantifying the enrichment.

Overall, these preliminary characterization approaches show that under the shear and impact forces applied during ball milling, the aggregated nanoparticles became more closely packed, while globally preserving their mean diameter and specific surface area. A possible re-arrangement of siloxane bonds was deduced from the slight modifications observed in σ_{as}(Si–O–Si) bands, and LG-SIMS analyses confirmed that the silica is ^{17}O-enriched to a level that specifically labels the silica outer-surface. We next turned to solid-state NMR to study the local structural changes between the Aerosil precursor and milled phases, and get more detailed insight into the enrichment of the silica surface.

Solid-state NMR investigation of structural changes for different BM durations

^{29}Si NMR analyses of the Aerosil precursor and the milled phases were first performed to study the Si–O–Si hydrolysis and bond rearrangement (Figures 2a and S4b). The ^{29}Si MAS NMR spectra of all compounds could be deconvoluted into three peaks, corresponding to Q^2 ($\underline{Si}(OSi)_2(OH)_2$), Q^3 ($\underline{Si}(OSi)_3(OH)$), and Q^4 ($\underline{Si}(OSi)_4$) environments.[12] The variation in the degree of siloxane condensation as a function of milling time (as calculated from the ^{29}Si NMR data) is shown in Figure S5, together with associated error bars. The result shows a small but noticeable decrease of siloxane condensation degree, which varies from 0.96% for Aerosil to 0.94% for BM_{15min}–SiO_2, the decrease was more pronounced during the first 5 minutes of milling. These changes in condensation degree might be simply explained by gradual hydrolysis of the siloxane bonds into silanols ("Si–O–Si + H_2O→2 Si–OH"). The slight decreases in the condensation degree are in line with the limited shift in σ_{as}(Si–O–Si) mentioned previously, and most certainly reflect a chain of hydrolysis and condensation reactions during milling, leading to Si–O–Si and Si–OH bond arrangements at the surface of the aggregated nanoparticles.

^{17}O NMR experiments were then carried out at these two milling times. Because oxygen-17 is a quadrupolar nucleus, signals are broadened by the quadrupolar interaction. When observing the central transition (as in our conditions), the

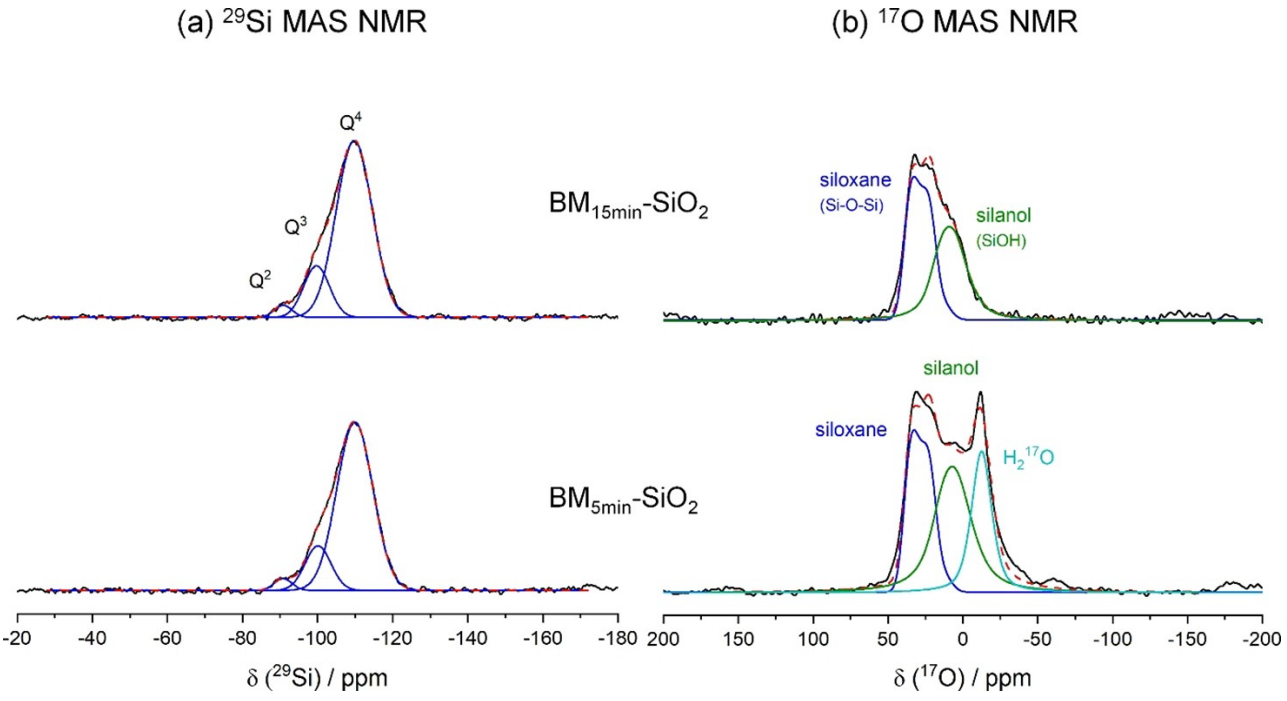

Figure 2. (a) ^{29}Si MAS NMR spectra (Bloch decay) of BM_{5min}–SiO_2 and BM_{15min}–SiO_2 (9.4 T, 5 kHz MAS). The experimental data are shown in black with overall fit in a red dashed line. The individual peaks were fitted using Gaussian lineshapes (blue), and assigned to Q^2, Q^3, and Q^4. The fitting parameters used here are consistent with the ^{29}Si{^{1}H} CPMAS spectrum of BM_{15min}–SiO_2 (see Figure S4). Samples for ^{29}Si NMR analyses were prepared using non-labeled H_2O. (b) ^{17}O MAS NMR spectra (Bloch decay) of BM_{5min}–SiO_2 and BM_{15min}–SiO_2 (18.8 T, 20 kHz MAS). The experimental data are shown in black with their overall fit in a red dashed line. The deconvolution peaks are assigned to siloxanes (blue), silanols (green), and $H_2{}^{17}O$ (cyan). The NMR parameters used for fitting are $\delta_{iso} = 42.0$ ppm, $C_Q = 5.2$ MHz, and $\eta_Q = 0.15$ for siloxanes, and $\delta_{iso} = 22.8$ ppm, and $C_Q = 5.1$ MHz, and $\eta_Q = 0.5$ for silanols. The water peak is fitted using a Gaussian lineshape with $\delta_{max} = -12.1$ ppm and FWHM = 16 ppm.

lineshape is dominated by the second-order quadrupolar interaction under magic-angle spinning (MAS). As the second-order quadrupolar broadening is inversely proportional to the Larmor frequency, the width of the lineshape decreases with increasing magnetic field strength, meaning that measurements at higher magnetic fields are preferable to achieve higher resolution.[36–39] Here, the first set of 1D ^{17}O MAS NMR spectra of BM_{5min}–SiO_2 and BM_{15min}–SiO_2 was thus recorded at 18.8 T (Figure 2b). At this field, while siloxane and silanol resonances still overlap,[18,33] a distinct resonance centered at −12.1 ppm is clearly observed for the BM_{5min}–SiO_2 phase, the ^{17}O chemical shift of which is consistent with water.[26,40] This resonance then disappears after 15 minutes of milling. Fast-MAS ^{1}H NMR analyses were performed, leading to a similar conclusion (Figure S6). For BM_{5min}–SiO_2, a relatively sharp and intense ^{1}H Lorentzian peak was observed at 4.2 ppm, which is consistent with physiosorbed water (this resonance overlapping the signals of the silanols on the silica surface).[13,41] For BM_{15min}–SiO_2, however, only a broad and less symmetric ^{1}H resonance centered at ≈5.5 ppm is observed, which is indicative of the predominance of hydrogen-bonded silanol groups. Given that both phases had been dried under similar conditions after 5 and 15 minutes of ball milling, it can be suggested that the distinct ^{17}O and ^{1}H NMR signatures arise from water molecules trapped within pores between silica particles, which have not yet had a chance to react with the silica surface during the first 5 minutes of milling, and could not be easily removed under vacuum. Regarding silanols and siloxanes, given that their ^{17}O resonances still overlapped at 18.8 T, additional analyses were required to achieve higher resolution and enable spectral deconvolutions.

The ^{17}O MAS NMR spectra of BM_{15min}–SiO_2 at three different magnetic fields (14.1, 18.8, and 35.2 T) are shown in Figure 3a. At ultrahigh magnetic field (35.2 T), the quadrupolar broadening is reduced even more drastically, and the ^{17}O signal was now separated into two clearly distinct resonances. The resonance centered at ≈38 ppm is attributed to oxygen atoms bridging silicon atoms in the siloxane bond (Si–O–Si) and the

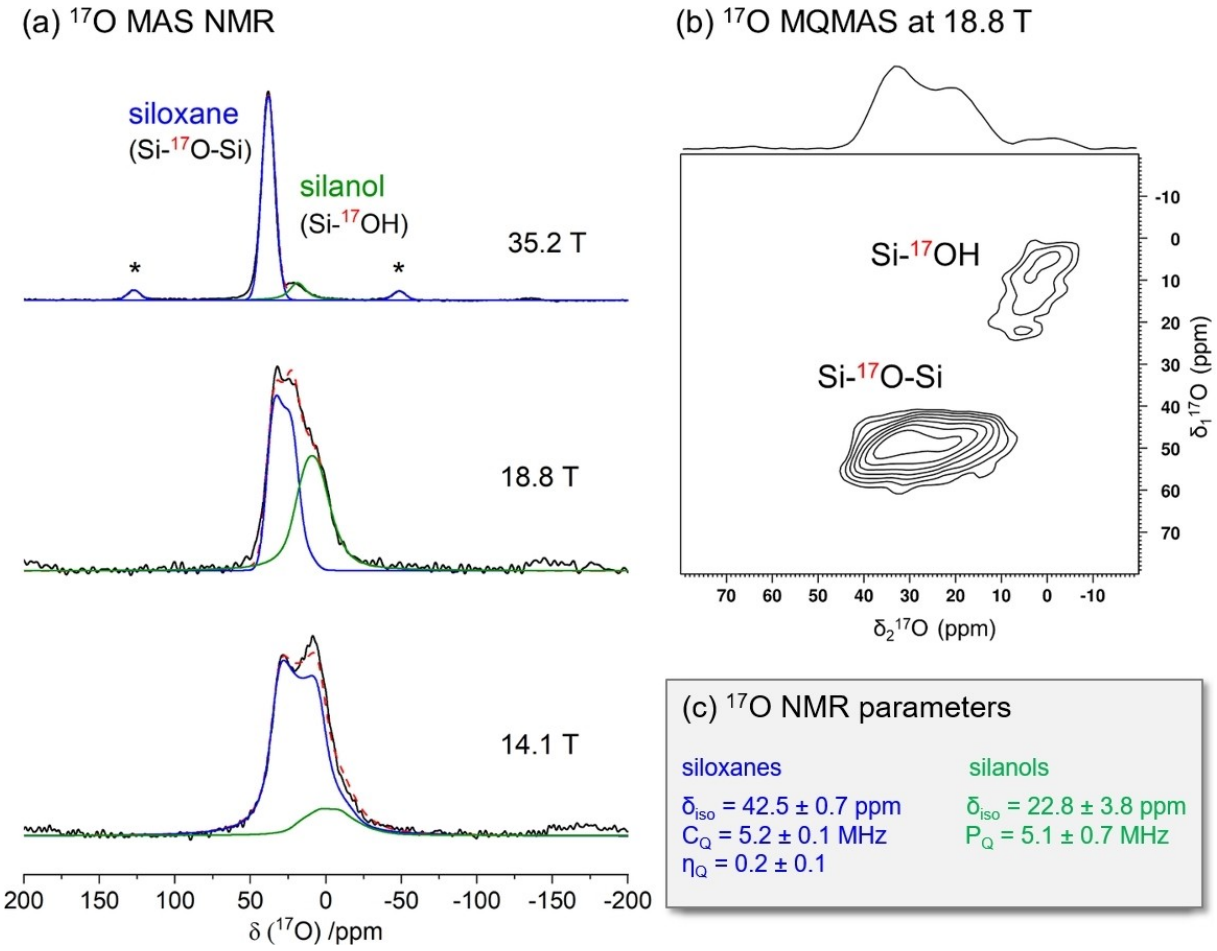

Figure 3. (a) ^{17}O MAS NMR spectra of BM_{15min}–SiO_2 (top) ^{17}O Bloch decay spectrum (14.1 T, 18 kHz MAS). (middle) ^{17}O MAS Bloch decay spectrum (18.8 T, 20 kHz MAS), and (bottom) ^{17}O polarization-enhanced spin-echo spectrum (35.2 T, 18 kHz MAS) * indicates spinning sidebands. A tentative deconvolution was performed using a same set of NMR parameters (δ_{iso} = 42.5 ± 0.7 ppm, C_Q = 5.2 ± 0.1 MHz, and η_Q = 0.2 ± 0.1 for siloxane, and δ_{iso} = 22.8 ppm, C_Q = 5.1 MHz, and η_Q = 0.5 for silanols). Exact C_Q and η_Q quadrupolar parameters could actually not be extracted for silanols, but rather a P_Q parameter could be obtained (as shown in Figure S7). The experimental data are shown in black with overall fit in a red dashed line. The deconvolution peaks correspond to siloxanes (blue) and silanols (green). (b) ^{17}O MQMAS spectrum of BM_{15min}–SiO_2 (18.8 T, 20 kHz MAS). The acquisition time is ≈2 h. (c) ^{17}O NMR parameters of siloxanes and silanols.

one at ≈20 ppm to oxygen atoms forming silanol groups (Si–OH).[18,26,33] The lineshapes of the siloxane and silanol resonances are nearly isotropic, suggesting the broadening of the peak is dominated by the chemical shift distribution instead of quadrupolar interaction at this field. These measurements allowed a deconvolution of the ^{17}O NMR data at the three fields to be performed (Figure 3).

It should be noted that different enriched siloxane/silanol ratios are observed in the spectra of BM_{15min}–SiO_2 shown in Figure 3a. We found that the ratio between ^{17}O signals of siloxanes and silanols represents the state of the sample at the moment of the measurement. The relative proportion of silanols was the lowest for the sample analyzed at 35.2 T, which had been synthesized over a month before the NMR. Moreover, we noticed that for BM_{15min}–SiO_2, this ratio changed from 70:30 to 82:18 after three months of storage in a freezer, even when the sample was only used for NMR experiments (Figure S8). This observation can be explained by the gradual back-exchange of the ^{17}O enriched Si–OH with non-labeled oxygen.[26] Consequently, although it could seem that the relative amount of enriched silanols decreases at longer milling times to the benefit of enriched siloxanes (Figure 2b), siloxane/silanol ratios could not be determined with high accuracy for BM_{5min}–SiO_2 and BM_{15min}–SiO_2 phases.

The complementary multiple-quantum MAS (MQMAS) spectrum of BM_{15min}–SiO_2 at 18.8 T is shown in Figure 3b. The acquisition time for recording the 2D MQMAS spectrum with a good signal-to-noise ratio was only ≈two hours, demonstrating that 15 minutes of ball milling can provide a ^{17}O labeling of the silica surface which is sufficient for performing high-resolution NMR spectroscopy including multidimensional experiments. The two resonances belonging to the siloxane and silanol groups were clearly resolved,[18,40] with NMR parameters consistent with those extracted from the deconvolutions of the 1D ^{17}O NMR spectra at three magnetic fields (Figure S9). Regarding siloxane bonds, only a small range of chemical shifts was observed (≈18 ppm span in the projection of the δ_1 dimension), while for silanols, a broader range in chemical shifts was found (≈30 ppm span in the δ_1 dimension). This result suggests that there are several different Si–OH environments in the sample, possibly involving various hydrogen-bonding schemes.

^{17}O MAS DNP investigation of the labeling of the silica surface

Having demonstrated that both ^{17}O enriched siloxanes and silanols are present after 15 minutes of milling, but that the overall labeling level is relatively low, it is legitimate to hypothesize that both types of bonds observed are mainly at the surface of Aerosil and have become enriched in ^{17}O (see above). This prompted us to turn towards DNP to look at surface oxygen sites. Indeed, with DNP, samples are most often impregnated with a solution of radicals, and then irradiated with microwaves, leading to the polarization transfer from unpaired electrons to nuclei.[42] When the samples are impregnated, DNP thus mostly enhances the sample's surface, and is well-suited to study the surface oxygen environments.[43–45] This was shown in the case of ^{17}O-enriched CeO_2 nanoparticles, where the first three layers could be detected and identified by DNP.[44]

Direct-polarization and indirect-polarization are complementary DNP methods: the former can be used to probe all oxygen sites at or close to the surface, while the latter to selectively detect the protonated oxygen sites.[21,44] In direct-polarization, ^{17}O is polarized directly by the nearby DNP radicals (assuming nuclear spin diffusion is quenched), while in indirect-polarization, ^{1}H nuclei are polarized first, and their polarization is then transferred to nearby ^{17}O atoms using cross-polarization (CP). In the case of silica, Perras et al. had shown the difference between direct-polarization and indirect polarization for the study of ^{17}O sites in surface-enriched mesoporous silica nanoparticles, with the former showing mainly siloxanes while the latter allowing for selective detection of silanols.[21]

Both methods were applied here on BM_{15min}–SiO_2 to probe the surface oxygen species (Figure 4). In the direct polarization experiment (Figure 4a), in the absence of microwave irradiation (μw off), the ^{17}O signal of milled silica was observed, which corresponds to overlapped siloxane and silanol resonances (at $B_0 = 14.1$ T). With microwave irradiation (μw on), the overall lineshape was enhanced. The difference spectrum between microwaves on and off corresponds to signals coming from the surface. Interestingly, the lineshape of all three spectra was found to be very similar, pointing out that both ^{17}O-enriched siloxane and silanols are present at the surface. To confirm these observations, a series of direct-polarization DNP experiments using different recycle delays were also performed (Figure S10). No strong changes in lineshape and the proportion of siloxane and silanols were observed.

In the indirect-polarization experiment (Figure 4b), a $^{17}O\{^{1}H\}$ DNP CPMAS analysis at a very short contact time (50 μs) was performed to probe the oxygen sites closest to protons. The signal observed without microwave irradiation comes predominantly from silanols.[21] This signal was then greatly enhanced with microwave irradiation. The difference spectrum showed the same lineshape for the spectra recorded with and without microwave irradiation as already noticed for the direct-polarization spectra.

In summary, direct and indirect-polarization DNP NMR results give complementary information regarding the surface oxygen sites including non-protonated and protonated species and showed that both ^{17}O signals of siloxane and silanol bonds could be enhanced by DNP, with no change in relative proportion with and without microwave irradiation. These DNP experiments thus fully agree with the selective formation of a ^{17}O-labeled silica surface.

High-resolution NMR analyses of surface oxygen sites

More details about different surface oxygen sites related to the hydrogen-bond network were investigated by a 2D ^{17}O–^{1}H correlation experiment. Previous works had shown that silica phases can be analyzed in detail using ^{17}O···^{1}H heteronuclear

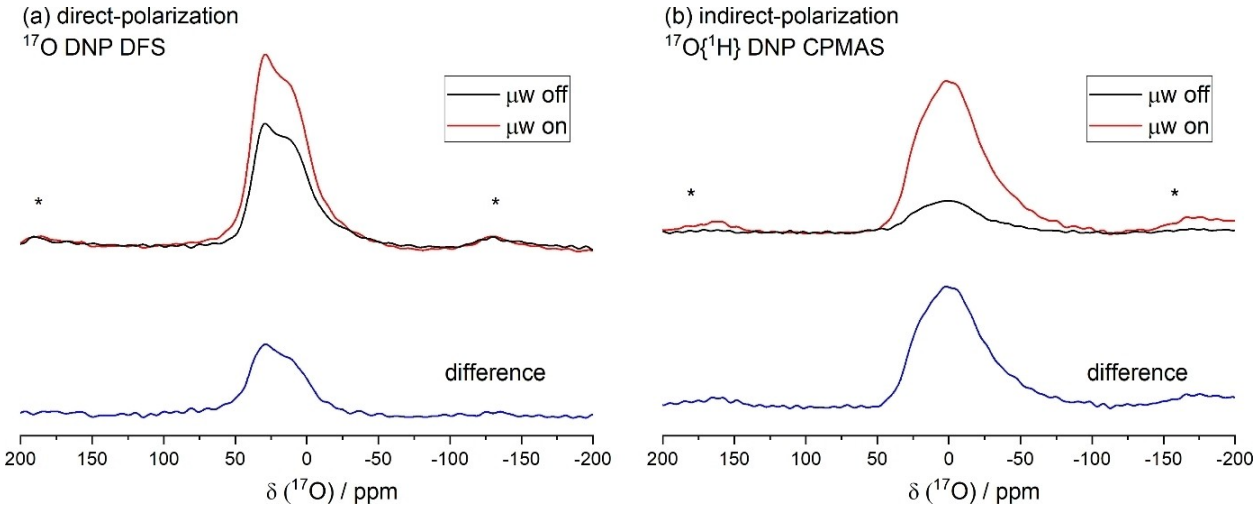

Figure 4. ^{17}O DNP NMR spectra of BM_{15min}–SiO_2 (14.1 T, 13 kHz MAS) (a) Direct-polarization experiments with (red) and without (black) microwave (μw) irradiation. ^{17}O DNP MAS NMR spectra recorded using DFS enhancement. The difference between μw on and off is in blue. Experimental time was ≈9 minutes. (b) Indirect-polarization experiments with (red) and without (black) microwave irradiation. ^{17}O{^{1}H} DNP CPMAS NMR spectra recorded with a contact time at 50 μs. * indicates spinning sidebands. Experimental time was ≈14 minutes per spectrum.

correlations based on dipolar and/or J couplings.[18,32,46,47] Here, the spatial proximities between ^{1}H and ^{17}O were probed by ^{17}O {^{1}H} D-HMQC (Dipolar- heteronuclear multiple quantum coherence) experiments (Figure 5). At a short-recoupling time (200 μs), only the closest hydrogen atoms can be observed which mainly correspond to O–H bonds, while at a longer recoupling time, more distant O···H interactions become visible. At a short recoupling time (τ_{rec} = 200 μs, Figure 5a), the main cross-peak (centered at $\delta(^{17}O)$ = 3.8 ppm) corresponds to Si–OH groups which correlate to ^{1}H signals spanning from ≈2 to 6 ppm. This wide range of ^{1}H chemical shifts suggests a variety of hydrogen-bonds around the silanols. Indeed, it is known that the ^{1}H chemical shift often reflects the strength of hydrogen-bonding interaction, with higher ^{1}H chemical shifts corresponding to stronger hydrogen-bonds.[7,19,48,49]

At a longer recoupling time (τ_{rec} = 1500 μs, Figure 5b), Si–OH groups show a clear correlation with a distinct proton at $\delta(^{1}H)$ = 2 ppm, which corresponds to isolated Si–OH groups according to the literature.[7,48] The fact that the isolated Si–OH groups have a more pronounced intensity at the longer recoupling time can be explained by their longer T_2 relaxation time than the other silanol groups.[32] Therefore, thanks to contrasts in ^{1}H and ^{17}O chemical shifts and relaxation times, this well-separated cross-peak for the isolated Si–OH could further allow specific studies of these chemical groups, even in the presence of a significant proportion of hydrogen-bonded silanols that otherwise mask their signal in the ^{1}H NMR spectra (as observed here in Figure S11). Another cross-peak shows that the siloxane signal (centered at $\delta(^{17}O)$ = 30 ppm) correlates to ^{1}H resonances spanning from $\delta(^{1}H)$ ≈2 to 6 ppm, which can be indicative of some siloxanes being hydrogen-bonded to silanols.

Overall, both short and long recoupling times bring evidence of a diversity of enriched silanol environments at the silica surface, and of a distribution of hydrogen-bonding, but with slight differences. The ^{1}H projection spectra for the two recoupling times are shown in Figure S11. At the short recoupling time, the signal is towards the lower chemical shift values suggesting a higher contribution of silanols forming weaker hydrogen-bonds, while the longer recoupling time shows an increased contribution of silanols more strongly hydrogen-bonded.

We further compared the surface structures of the samples enriched by LAG for 5 and 15 minutes. The 2D ^{17}O{^{1}H} D-HMQC experiment performed with a long recoupling time on BM_{5min}–SiO_2 is shown in Figure S12. Similar cross-peaks were observed as in BM_{15min}–SiO_2, corresponding to isolated silanols, and the correlation between siloxanes and surface OH groups. Hence, it appears that all the different types of oxygen sites start getting enriched during the first 5 minutes of milling, and with longer milling times, more of each type of oxygen site gets labeled in ^{17}O, due to the increasing bond rearrangements caused by the impact and shear forces, which lead to the increase of the ^{17}O enrichment level.

The ^{17}O chemical shifts and quadrupolar parameters of Si–OH groups are known to be sensitive to local structural variations. In a previous study,[18] two ^{17}O labeled silica surfaces obtained by varying heat treatments showed differences in ^{17}O chemical shift of silanols, with the ^{17}O silanol signature in the silica phase prepared at a higher temperature shifting to a lower frequency. In our case of a milled silica phase isolated without any heat treatment, the silanol bonds show a broad distribution in both ^{17}O and ^{1}H chemical shifts, which may be explained by the presence of a diverse hydrogen-bonded network at the surface. Furthermore, looking at the data obtained for short recoupling times, it seems that the ^{17}O NMR shifts correlate to the ^{1}H chemical shift: a trend of silanol distribution is observed in the ^{17}O{^{1}H} D-HMQC spectra (red

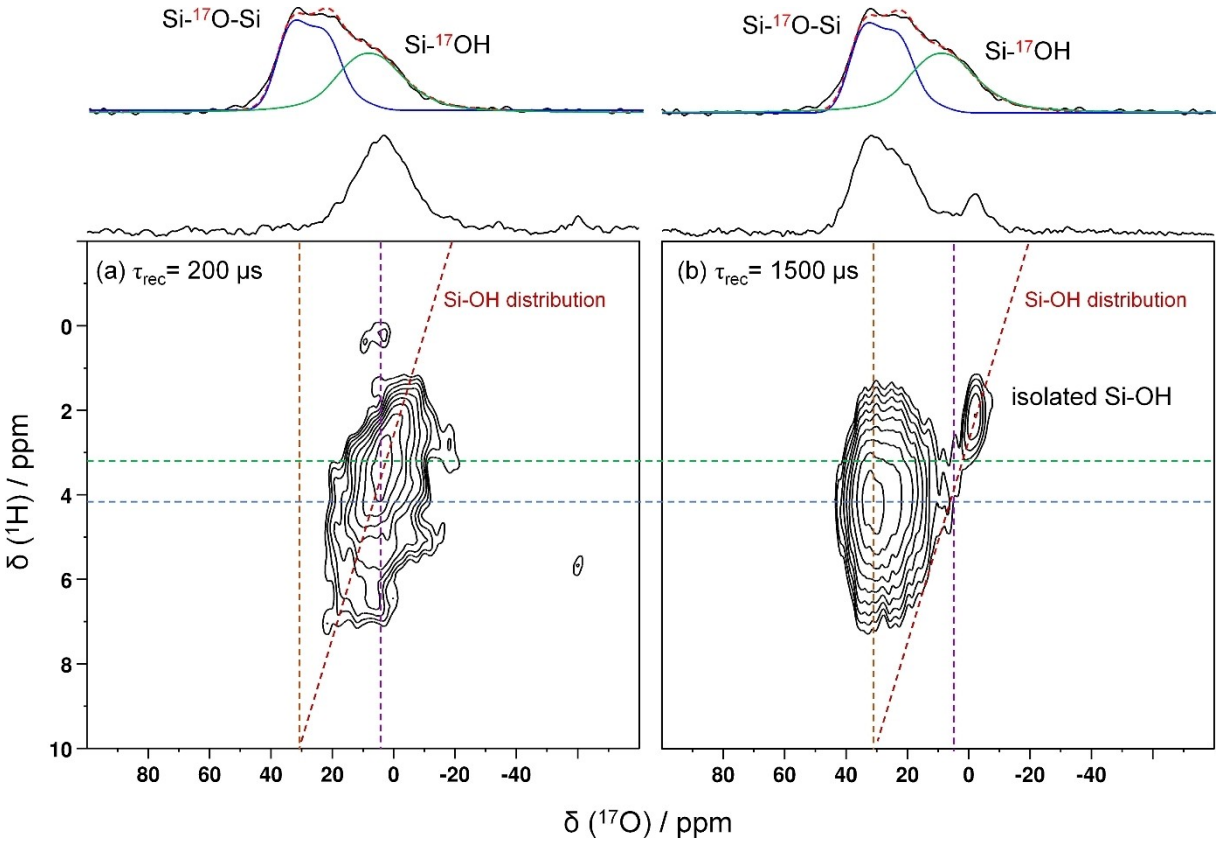

Figure 5. $^{17}O\{^{1}H\}$ D-HMQC of BM_{15min}–SiO_2 (18.8 T, 20 kHz MAS) at different recoupling times, with the ^{17}O 1D MAS NMR spectrum recorded at the same field shown just above. (a) recoupling time (τ_{rec}) of 200 µs; (b) recoupling time (τ_{rec}) of 1500 µs. Dashed lines are provided as a guide to compare spectra recorded at both recoupling times. The red dashed line (diagonal) for $\tau_{rec} = 200$ µs suggests a correlation between the ^{17}O and ^{1}H chemical shifts in the Si–OH distribution (and was also plotted for $\tau_{rec} = 1500$ µs).

dashed line in Figures 5a and 5b). A similar trend between ^{1}H and ^{17}O chemical shifts of silanols can be retrieved from the *ab Initio* study of a model of the surface for amorphous silica (Figure S13).[5] Therefore, there is information to get on the silanol distributions and on the nature of hydrogen-bonded networks from these 2D $^{17}O\{^{1}H\}$ D-HMQC spectra. Combined with the easy ^{17}O labeling of the silica surface, this opens new perspectives in the characterization of hydrogen-bonded silanols that merits further experimental and theoretical investigations to better match the analyzed surface with the modeled surface and to explain the ^{1}H–^{17}O correlation trend observed.

^{17}O NMR and DNP investigation of the reactivity of the surface-enriched silica phase

The surface ^{17}O-labeled silica phase prepared using the newly developed enrichment method shows both ^{17}O-enriched siloxane and silanol bonds. This phase is thus well suited for studying the reaction mechanisms involved when making more complex mixed oxides in the solid-state by ball milling reactions. Previously, we had shown that bond rearrangements occur when mixing SiO_2 and Ti^*O_2 under dry-milling conditions after only three minutes of ball milling.[33] The ^{17}O-enriched siloxane signature had been observed (Figure 6a, $TiO^*_2 + SiO_2$ case). In addition, a new resonance centered at ≈220 ppm was also noticed, the ^{17}O chemical shift of which is in the range expected for Ti–OH and Si–O–Ti bonds.[29,50] Yet, no clear assignment of this resonance was then made.

We decided to go into more depth in the study of this reaction, taking advantage of this newly developed BM protocol to produce Si^*O_2 with a high surface area from Aerosil. To complement the previous work, two phases were prepared using different labeled precursors, but with the same milling conditions as previously (i.e. three minutes at a frequency of 25 Hz): (i) one ^{17}O-enriched phase was prepared from Si^*O_2 and TiO_2 (anatase) and (ii) one ^{17}O-enriched phase was prepared from Ti^*O_2 and Si^*O_2. No difference was observed between these phases in PXRD (Figure S14a). From the TEM image of the ^{17}O-enriched phase of Ti^*O_2 and Si^*O_2, the two oxide particles appear to be homogeneously mixed (Figure S14b).

Each mixed-phase was analyzed by high field ^{17}O MAS NMR and ^{17}O DNP NMR (Figure 6). In the case of the ^{17}O-enriched phase isolated from mixing TiO_2 and Si^*O_2, the ^{17}O resonance centered at 24 ppm corresponds to the enriched precursor Si^*O_2 (Si–^{17}O–Si groups). The ^{17}O resonance centered at 556 ppm was observed only after milling (Figure 6b), and its ^{17}O

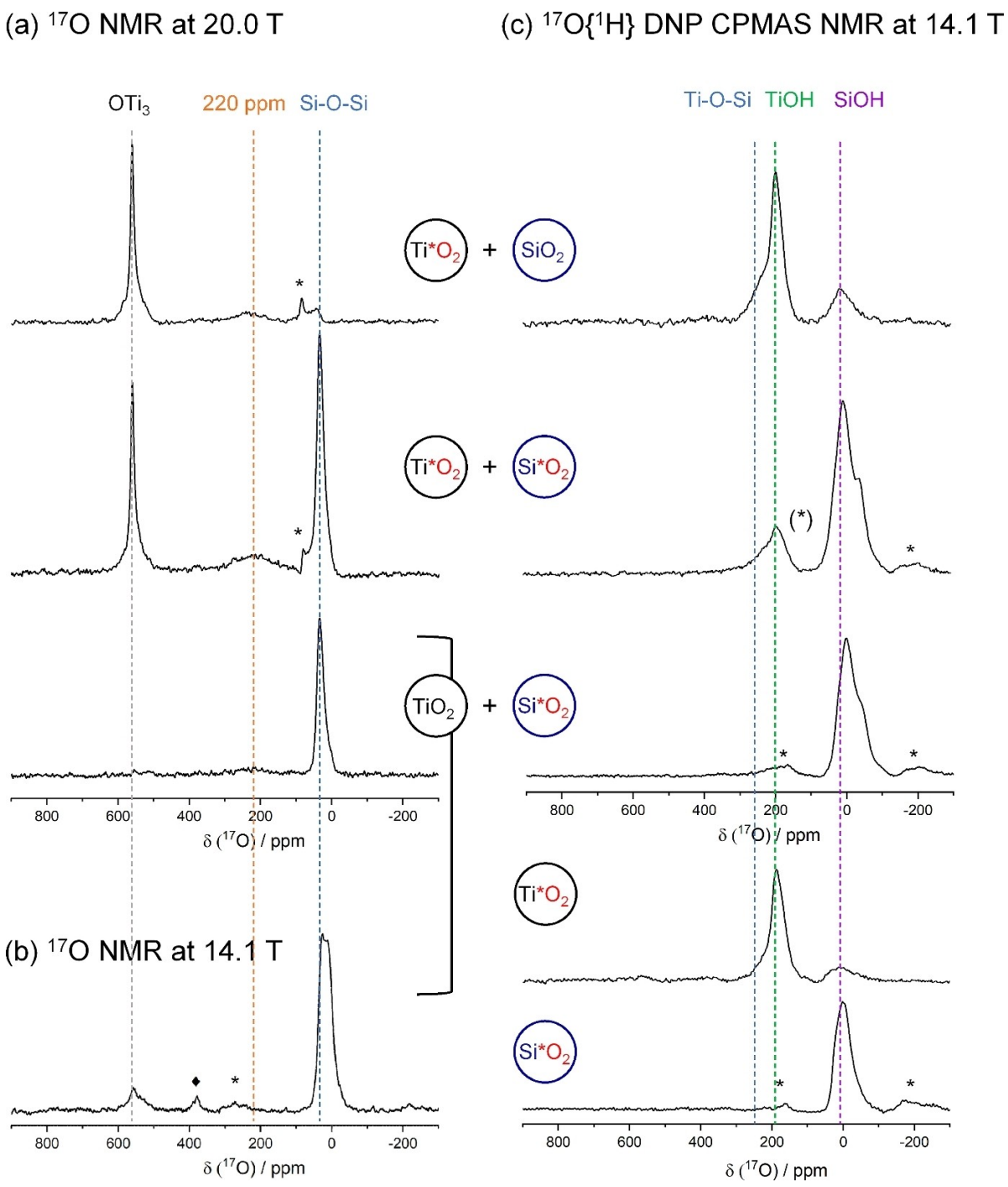

Figure 6. (a) ^{17}O polarization-enhanced spin-echo NMR spectra of $Ti^*O_2 + SiO_2$ [33], $Ti^*O_2 + Si^*O_2$, and $TiO_2 + Si^*O_2$ (20.0 T, 55 kHz MAS). The temperature of ^{17}O NMR spectra of $Ti^*O_2 + Si^*O_2$, and $TiO_2 + Si^*O_2$ mixtures was controlled at 0 °C. (b) ^{17}O DFS NMR spectrum of $TiO_2 + Si^*O_2$ (14.1 T, 20 kHz MAS) (c) ^{17}O {^1H} DNP CPMAS NMR spectra of $Ti^*O_2 + SiO_2$, $Ti^*O_2 + Si^*O_2$, and $TiO_2 + Si^*O_2$, Ti^*O_2 [33], and Si^*O_2. The contact time was 50 μs. (14.1 T, 13 kHz MAS). * indicates spinning sidebands and ♦ indicates zirconia rotor.

chemical shift corresponds to OTi_3 environments. This shows OTi_3 sites can be enriched by only three minutes of dry milling with the presence of ^{17}O-labeled silica, which suggests that fast bond rearrangements occur, as previously observed in the $\{Ti^*O_2 + SiO_2\}$ case. Fast MAS ^{17}O NMR spectra of mixed oxides were recorded at a high field to better observe the region around 200 ppm (Figure 6a). A broad weak signal centered at ≈220 ppm was observed in all three mixed oxides prepared from different precursors, which seemed relatively more intense in the case of a ^{17}O-enriched phase prepared from $\{Ti^*O_2 + Si^*O_2\}$, as would be expected in the presence of more Si–O–Ti bonds. As the signal of interest at ≈220 ppm was too weak for

further NMR analyses, we applied DNP to enhance the NMR sensitivity. Previously, we had successfully detected the Ti–OH groups at the surface of the precursor Ti^*O_2 via $^{17}O\{^1H\}$ DNP CPMAS, while their signal was too weak to be detected using conventional solid-state NMR (Figure 6c).[33]

Here, direct-polarization and indirect-polarization experiments were both performed to examine the surface oxygen environments in the mixed oxide phases. Unfortunately, the signal centered at ≈220 ppm was not significantly enhanced in the case of direct-polarization experiments and overlapped with spinning sidebands (Figure S15). In contrast, the indirect-polarization experiments ($^{17}O\{^1H\}$ DNP CPMAS NMR) were more informative. The spectra of the three phases with a short contact time are shown in Figure 6c. Strong ^{17}O NMR signals are observed in the DNP spectra of the ^{17}O-enriched phase made from $\{Ti^*O_2 + SiO_2\}$. The weak ^{17}O signal centered around 200 ppm is now greatly enhanced thanks to DNP and suggests the presence of several overlapping oxygen environments. More specifically, it could be deconvoluted into two contributions, centered at 187 and 206 ppm (Figure S16). The peak maximum at 186 ppm was assigned to Ti–OH since it is consistent with the observed Ti–OH group in the Ti^*O_2 precursor,[33] and with the literature.[51] The peak centered at 206 ppm could correspond to the Si–O–Ti bonds based on its chemical shift.[29,50] This signal was also observed in the ^{17}O-enriched phase prepared from $\{Ti^*O_2 + Si^*O_2\}$, but with a different relative intensity, which further confirms that this shoulder most likely belongs to the Si–O–Ti bond. As the Ti–OH and Si–O–Ti sites were enhanced by DNP, these two species are likely to be close to radicals that are present on the surface.

Complementary $^{29}Si\{^1H\}$ DNP CPMAS NMR analyses were performed on the ^{17}O-enriched phase resulting from the $\{Ti^*O_2 + Si^*O_2\}$ mixture. The ^{29}Si signal could be deconvoluted into Q^2, Q^3, and Q^4 peaks. The linewidth of the Q^2 and Q^3 peaks was broader than those of the precursor Si^*O_2 (BM_{15min}–SiO_2) (Figure S17). A similar broadening of the Q^2 and Q^3 sites had been reported in the literature of mixed oxides of silica and titania, in which the presence of Si–O–Ti had been evidenced.[27,52]

In summary, the NMR and DNP analyses performed on three phases prepared from different mixtures of labeled precursors ($Ti^*O_2 + SiO_2$, $Ti^*O_2 + Si^*O_2$, and $TiO_2 + Si^*O_2$) enabled not only demonstration of the utility of having access to a ^{17}O-labeled silica phase to study reaction mechanisms between solids, but more importantly to identify interfacial bonds. Thanks to DNP, direct evidence of the formation of Si–O–Ti bridges at the interface between the two oxide particles could be obtained.

Conclusion

Selective surface ^{17}O labeling of fumed silica was successfully achieved for the first time by using a user-friendly experimental approach involving mechanochemistry. More specifically, by using the LAG approach with a vertical mixer mill and hardened stainless steel reactors and milling balls, the enriched material was formed with only microliter amounts of ^{17}O-labeled water. The textural changes of milled silica were studied before and after milling, showing the possibility of tailoring the pore sizes of ^{17}O-enriched silica by using different milling times. The absolute ^{17}O enrichment level (≈5.3%) was determined by LG-SIMS, which allowed us to estimate that only the outer surface of the silica particles had been enriched. The level of enrichment of a thin outer shell of the aggregated nanoparticles was sufficient to perform high-resolution NMR such as ^{17}O MQMAS and $^{17}O\{^1H\}$ D-HMQC experiments in a reasonable time. These NMR results show that both siloxanes and silanols were enriched by only 5 minutes of milling. Moreover, different types of silanols were enriched including hydrogen-bonded silanols and isolated silanols. A trend was observed between ^{17}O and ^1H chemical shifts for the silanols, which could be useful for future studies of the characterization of hydrogen-bonded silanols and the modeling of silica surfaces. Moreover, future investigations would be worth performing using probe molecules or by modifying the silica surface to determine if these ^{17}O enriched isolated silanols are accessible.[3,53] Additionally, the surface-enriched silica prepared here could be used to investigate the interface of a ^{17}O-enriched phase of titania and silica, and Si–O–Ti sites could be identified at the interface of two oxides thanks to DNP enhancement. Such information is highly valuable for developing a detailed understanding of reaction mechanisms by ball milling, by pointing out the bonds which form between reacting particles, and could not have been achieved in absence of isotopic labeling. Finally, extensions of these ^{17}O-labeling procedures to other amorphous or micro/nano-crystalline silica phases (e.g. quartz – Figure S2b) have also started to be examined.

Experimental Section

Reagents and equipment: SiO_2 (Aerosil 200, Degussa, 180 m^2/g, aggregated nanoparticles of ≈12 nm diameter) and TiO_2 (St-Gobain Norpro, anatase phase, 150 m^2/g) were used as main oxide precursors. The porous TiO_2 precursor, initially in the form of cylindrical monoliths (≈1 cm long, ≈0.3 cm diameter), was pre-ground into a fine powder using an agate mortar and pestle before use. A quartz phase (BCR-066; particle size: 0.35–3.5 μm) was also enriched once in ^{17}O for comparison to Aerosil (Figure S2b). ^{17}O-enriched water was purchased from CortecNet. The isotope composition of this water is ≈90.4% of ^{17}O. TEKPol and d_2-tetrachloroethane were purchased from Cortecnet. Tetrabromomethane was purchased from Sigma-Aldrich.

Ball milling experiments were carried out either using a Retsch Mixer Mill 400 (MM400) apparatus or a Fritsch P23 vertical mixer mill. For the P23 mixer mill, the hardened stainless steel jar and balls were used. For the MM 400 mixer mill, the stainless steel jar with a screw-top lid (used in LAG) or push-fit lid (used in dry milling) and stainless steel balls were used.

Isotopic labeling reactions by using mechanochemistry

Synthesis of ^{17}O labeled oxides by liquid-assisted grinding: Before ball milling experiments, all oxide precursors were dried under vacuum using a Schlenk line at ≈0.6 mbar for 4 h at room temperature. The experimental conditions for each ^{17}O enriched sample are listed in Table 1. In all experiments, first, the milling balls (10 mm diameter) were introduced into a milling jar (10 mL

Table 1. Experimental conditions for liquid-assisted grinding and dry milling experiments discussed in the manuscript.

^{17}O-labeling by liquid-assisted grinding Sample	Mixer mill	Oxide precursor [mg]	$H_2{}^{17}O$ [μL]	Number of balls	Milling time [min]	Color after milling	Mass recovered before vacuum [mg]	Mass after 15 min vacuum [mg]
BM_{5min}–SiO_2	P23	SiO_2 (Aerosil) (100.9 ± 0.2)	30	2	5	White	124 ± 2 (n = 2)[a]	97 ± 1 (n = 2)
BM_{15min}–SiO_2	P23	SiO_2 (Aerosil) (100.7 ± 0.2)	30	2	15	White	126 ± 1 (n = 2)	99 ± 4 (n = 2)
Ti^*O_2[33b]	MM400	TiO_2 (50.5 ± 0.3)	11	1	15	light grey	38 ± 1 (n = 3)	34 ± 1 (n = 3)
Dry milling Sample	Mixer mill	TiO_2 precursor [mg]	SiO_2 precursor [mg]	Number of balls	Milling time [min]	Color after milling	Mass recovered [mg]	
$Ti^*O_2 + SiO_2$[33]	MM400	Ti^*O_2 (28.7 ± 0.1)	SiO_2 (Aerosil) (21.8 ± 0.4)	1	3	light grey	43 ± 1 (n = 2)	
$TiO_2 + Si^*O_2$	MM400	TiO_2 (28.6 ± 0.2)	Si^*O_2 (BM_{15min}–SiO_2) (21.8 ± 0.3)	1	3	light grey	39 ± 2 (n = 2)	
$Ti^*O_2 + Si^*O_2$	MM400	Ti^*O_2 (28.7)	(BM_{15min}–SiO_2) (21.4)	1	3	light grey	42 (n = 1)	

[a] In the table, n is the number of repetitions performed for each experiment. [b] the ^{17}O-labeling in this Ti^*O_2 precursor was estimated < 14%, considering the milling conditions used here and our previous work.[33]

volume) followed by the dried precursors. Lastly, $H_2{}^{17}O$ was added to the milling jar, using a 1:1 molar ratio between the oxide precursor and $H_2{}^{17}O$. All samples were milled using a mixer mill with a frequency set to 25 Hz. After milling, the samples were recovered by gentle scratching of the jar and milling balls with a spatula, followed by drying under vacuum at ≈0.08 mbar at room temperature for 15 min to remove residual water. Dried samples were stored in glass vials (caps covered with parafilm), which were placed in a freezer in a container with drying beads to prevent humidity. Before any characterization or further analysis, samples were taken out for 30 min to warm up to room temperature.

It is worth noting that for the milling of silica, using the P23 mill mixer at 25 Hz with the Fritsch hardened stainless steel milling equipment had more advantages in comparison to the MM400 equipment. Firstly, less contamination (e.g., Fe, Cr) from the reactor and milling balls was observed. Secondly, the powder recovery was more straightforward from the P23 jar compared to MM400. Based on our observation, the recovered mass was often found to be lower after scratching the milling jar from a MM400 mixer mill than from a P23 mixer mill.

Dry milling of TiO_2 and SiO_2: The ^{17}O enriched phases resulting from the mixing of TiO_2 and SiO_2 were prepared by dry milling reaction following our previously published procedure.[33] In brief, the oxide precursors were dried prior to use as described in the previous section. The two oxides, taken in a 1:1 molar ratio, were then mixed manually together by simple shaking before introducing them into the milling jar. The samples were then milled, recovered by scratching and stored following the same procedure as described above. Here, samples were not dried under a vacuum after retrieving them from the milling jar. The experimental conditions for each ^{17}O enriched mixed-oxide sample are listed in Table 1.

It should be noted that the initial state of the three mixtures of powders (before dry milling) are different. Indeed, the starting materials used (Aerosil and anatase) come out with different textures after LAG. Hence, their reactivity in dry milling with respect to the other oxide could be slightly different, depending on whether they have been pre-labeled in ^{17}O or not.

Materials characterization

Powder X-ray Diffraction (PXRD): Powder XRD analyses were performed on a X'Pert MPD diffractometer using CuKα_1 radiation (λ = 1.5406 Å) in a Bragg-Brentano scanning mode. The operation voltage and current were at 40 kV and 25 mA. The diffractograms were recorded between 5 and 60°, with a step of 0.016°.

Infrared spectroscopy (IR): IR spectra were carried out on a Perkin Elmer Spectrum 2 FTIR instrument using the attenuated total reflectance (ATR) measurement mode (diamond crystal). The wavenumber range analyzed was 500–4000 cm^{-1}, and the optical resolution of the instrument was 0.5 cm^{-1}.

Energy-dispersive X-ray spectroscopy (EDXS) Analyses: EDXS analyses were performed on a Zeiss Evo HD15 scanning electron microscope equipped with an Oxford Instruments X–MaxN SDD 50 mm^2 EDXS detector. Samples were prepared by depositing the silica powders on a double-sided carbon tape and then metalized with carbon before measurements.

Transition electron microscopy (TEM): TEM experiments were carried out on a LaB6 JEOL 1400 Plus electron microscope operating at 100 kV. The TEM samples were prepared by depositing a dispersed suspension of powders (silica and ^{17}O enriched phase of $Ti^*O_2 + Si^*O_2$) in water onto carbon-supported copper grids and left to dry before measurements.

N_2 adsorption/desorption isotherms: N_2 volumetric analyses were conducted by physisorption of N_2 using a Tristar instrument (Micromeritics, Norcross, GA). Samples were degassed at 150 °C under vacuum overnight before measurements. Here, the samples analyzed corresponded to silica phases milled for different times (between one and fifteen minutes) in the presence of *non-labeled* water, using the conditions described above (P23 mixer mill, 25 Hz). Specific surface areas were derived from the isotherms using the Brunauer-Emmett- Teller (BET) method.[54] Errors on the surface areas for samples prepared under similar conditions were estimated to ± 20 $m^2 g^{-1}$. The distribution in pore diameters was plotted as a function of the pore volume (Figure S1d), by analyzing the desorption data using the Barrett-Joyner-Halenda (BJH) method.[55]

Large-geometry secondary-ion mass spectrometry (LG-SIMS): The starting Aerosil material and the ^{17}O enriched SiO_2 powders prepared by LAG (BM_{5min}–SiO_2 and BM_{15min}–SiO_2) were first pelletized and then embedded into indium alloy using a hydraulic press, in order to minimize sample degassing and improve electric conductivity at the surface of the sample mount. The embedded silica pellets were sputtered by a thin layer of gold before being placed into the high vacuum chamber of the LG-SIMS instrument. An in-house Aerosil reference material, previously characterized for its O-isotopes composition using an independent technique (see Supporting Information) was also embedded in indium and coated with gold, to be analyzed under similar conditions, and evaluate the extent of mass instrumental fractionation. A reference quartz sample (Bresil, for which $\delta^{17}O = 4.99‰$ and $\delta^{18}O = 9.60‰$) was also analyzed before and after sample analyses in order to perform instrument calibrations and alignments, and to verify the stability of the settings throughout the measurement session.

LG-SIMS experiments were carried out at the French national facility of the CRPG in Nancy on a CAMECA IMS 1280 HR ion microprobe. A $^{133}Cs^+$ primary ion beam was used, and secondary ions were extracted, allowing ^{16}O, ^{17}O, and ^{18}O to be monitored at a mass resolution of >2000. The instrument has been recently upgraded with high sensitivity faraday cups (FC $10^{12}\,\Omega$ amplifiers, as described by Bouden et al.)[35] This new type of collector offers optimal performances for secondary ion intensities varying from 1 to 2 x 10^6 count per second, which correspond to the typical range of ^{17}O measured in the present study. These conditions significantly improve the statistical errors (within spot uncertainties <0.2 ‰ 2σ, as shown in Figure 3. of the recent study by Bouden et al.)[35] associated with the collection of minor masses while working at high resolution. Data were acquired in both mono-collection (i.e. peak jumping) and multicollection (i.e. simultaneously) modes, in order to identify the best analytical protocol. Both settings return comparable analytical precision and provide identical results.[35]

For each sample, average $^{17}O/^{16}O$ ratios were determined by analyzing a minimum of three different zones of the surface and recording 30 cycles for each zone. The isotopic ratios reported herein (together with the corresponding standard deviations) correspond to an average over the different points of the surface which were analyzed, as shown in Table S1 (Supporting Information). For BM_{5min}–SiO_2, absolute ^{16}O, ^{17}O, and ^{18}O content were extracted from mono-collection mode data (and were found to be consistent with multi-collection mode analyses).

Solid-state NMR

1D ^{17}O NMR experiments: ^{17}O NMR spectra were recorded at multiple magnetic fields ($B_0 = 14.1$ T, 18.8 T, 20.0 T, and 35.2 T) in different NMR facilities, depending on the samples. ^{17}O chemical shifts were referenced using tap water at 0.0 ppm or to D_2O at −2.7 ppm.

At 14.1 T, ^{17}O MAS NMR spectra were acquired on a Varian VNMRS spectrometer using Varian 3.2 mm HX or HXY probes, or a PhoenixNMR HXY probe operating at a ^{17}O frequency of 81.31 MHz and ^1H frequency of 599.82 MHz. The spinning frequency was controlled at 16 kHz without temperature regulation. The double frequency sweep (DFS) was used for ^{17}O signal enhancement.[56] The parameters were as follows: DFS pulse of 500 μs (RF ≈ 10 kHz), swept between 200 and 80 kHz, and followed by an excitation pulse of 1.0 μs. For the ^{17}O MAS (Bloch decay) NMR experiments, a 2.0 μs pulse was used. The pulse was calibrated using the nutation curve of liquid water, for which the 90° pulse was 6.0 μs (RF 41.6 kHz).

At 18.8 T, ^{17}O MAS NMR spectra were acquired on a Bruker Avance NEO NMR spectrometer equipped with a 3.2 mm HX probe operating at a ^{17}O frequency of 108.46 MHz and ^1H frequency of 800.12 MHz. The spinning frequency was controlled at either 16 or 20 kHz without temperature regulation. The ^{17}O MAS (Bloch decay) NMR experiment was performed using a 0.75 μs pulse. The pulse was calibrated considering the nutation curve of liquid water, for which the 90° pulse was 4.6 μs (RF 54 kHz).

At 20.0 T, ^{17}O MAS NMR spectra were acquired on a Bruker Avance NEO NMR spectrometer equipped with a 1.3 mm HX probe operating at a ^{17}O frequency of 115.26 MHz and ^1H frequency of 850.23 MHz. The spinning frequency was controlled at 55 kHz and the temperature regulation unit was set to 0 °C. The ^{17}O polarization-enhanced spin-echo (WURST-echo) experimental details can be found below.[56]

At 35.2 T, ^{17}O MAS NMR spectra were acquired on a Bruker Avance NEO NMR spectrometer equipped with a 3.2 mm MAS single-channel probe operating at a ^{17}O frequency of 203.36 MHz. The spinning frequency was controlled at 18 kHz without temperature regulation. The experimental parameters for each ^{17}O experiment are listed in Table S3. The polarization-enhanced spin-echo spectra were recorded using a WURST pulse for satellite-transition inversion/saturation (1 ms pulse, set at 150 kHz offset),[56] followed by solid 90° and 180° pulses of 4.4 and 8.8 μs, and with the echo delay set to 1 rotor period.

Additional acquisition parameters (including recycle delays and number of scans) can be found in Table S3.

$^{17}O\{^1H\}$ D-HMQC and ^{17}O MQMAS NMR: $^{17}O\{^1H\}$ D-HMQC NMR spectra and ^{17}O MQMAS spectra were recorded at 18.8 T using a Bruker Avance NEO NMR spectrometer equipped with a 3.2 mm HX probe operating at a ^{17}O frequency of 108.46 MHz and ^1H frequency of 800.12 MHz. The ^{17}O pulse was calibrated using the nutation curve of water, for which the 90° pulse was 4.6 μs (RF 54 kHz). For $^{17}O\{^1H\}$ D-HMQC experiments,[57] two experimental conditions were used. The spinning frequency was set to 20 kHz without temperature regulation for BM_{15min}–SiO_2, and to 16 kHz with temperature regulated at 0 °C for BM_{5min}–SiO_2. The conditions used were as follows for BM_{15min}–SiO_2 (BM_{5min}–SiO_2): the ^{17}O initial central transition (CT) enhancement was performed using a 2 ms (1 ms) long ssQFS[58] pulse with a quadruple frequency sweep of 20 kHz centered at ±180 kHz and ±360 kHz offset (16 kHz centered at ±160 kHz and ±320 kHz offset), a maximum RF field of 9 kHz (24 kHz), and a WURST-100 amplitude envelope (WURST-10). The ^{17}O CT selective 90° and 180° pulses were 8.0 and 16.0 μs long (RF field ≈ 10 kHz) for BM_{15min}–SiO_2, and 10.0 and 20.0 μs long (RF field ≈ 7.5 kHz) for BM_{5min}–SiO_2. The 90° pulse on ^1H was 2.3 μs for both BM_{15min}–SiO_2 and BM_{5min}–SiO_2. The duration of $SR4_2^1$ recoupling on ^1H with 40 kHz RF field was set to 200 and 1500 μs for both samples.[59]

^{17}O MQMAS spectrum was recorded by split-t_1 shifted-echo MQMAS experiment using FAM–N reconversion pulses. The spinning frequency was controlled at 20 kHz without temperature regulation. The FAM–N pulses were optimized using Matlab/Simpson procedure developed by Colaux et al.[60,61] for sites with $C_Q / \eta_Q = 5$ MHz / 0 and an RF field of 70 kHz, leading to the use of 4 pulses for 3Q to 1Q reconversion of length 1.8, 1.45, 1.0, and 0.7 μs. The excitation pulse was 3.7 μs (RF field 70 kHz) and the 180° pulse was set to 14.0 μs (RF field 10 kHz). ^1H decoupling (RF field 105 kHz) was used during t_1 and t_2 (SPINAL-64 scheme).[62]

Additional acquisition parameters for both samples can be found in Table S3.

^{17}O polarization-enhanced spin-echo NMR experiments at high spinning speeds: At 20.0 T, ^{17}O MAS NMR spectra were acquired on a Bruker Avance NEO spectrometer equipped with a 1.3 mm HXY probe operating at a ^{17}O frequency of 115.26 MHz and ^{1}H frequency of 850.23 MHz. The same acquisition conditions were used as in our previous study.[33] The ^{17}O pulses were calibrated using the nutation curve of liquid water, for which the 90° pulse was 15.0 μs (RF 17 kHz) The spinning frequency was controlled at 55 kHz and the temperature unit was set to 0 °C. The ^{17}O satellite transitions were saturated with a 655 μs long WURST shaped pulse (1 W power) applied at an offset of twice of the spinning frequency (110 kHz) before the echo pulse sequence with an echo time of one rotor-period and with the 90° and 180° pulses set to 4 and 8 μs respectively. The other acquisition parameters (including recycle delays and number of scans) can be found in Table S3.

^{1}H MAS NMR experiments: ^{1}H Hahn-echo fast MAS NMR spectra were recorded at 14.1 T using a Varian VNMRS spectrometer equipped with a PhoenixNMR HXY probe operating at a ^{17}O frequency of 81.31 MHz and ^{1}H frequency of 599.82 MHz. The ^{1}H 90° and 180° pulses were set to 5.0 and 10.0 μs respectively. The spinning frequency was controlled at 55–60 kHz without temperature control, depending on the sample. The echo delay was set to 250.0 μs (15 rotor periods for 60 kHz and 14 rotor periods for 55 kHz). ^{1}H chemical shifts were referenced using adamantane as a secondary reference at 1.8 ppm. Additional acquisition parameters (including recycle delays) can be found in Table S3.

^{29}Si MAS NMR experiments: ^{29}Si MAS NMR spectra were recorded at 9.4 T using a Varian VNMRS 400 MHz spectrometer equipped with a Varian 7.5 mm HX probe operating at a ^{29}Si frequency of 79.46 MHz and a ^{1}H frequency of 399.92 MHz. The spinning frequency was set to 5 kHz without temperature control. The ^{29}Si NMR Bloch decay experiments used a small flip angle ($\pi/6$) pulse and with SPINAL-64 ^{1}H decoupling during acquisition (RF ≈25 kHz). The $\pi/6$ pulse was set to 2.0 μs. ^{29}Si{^{1}H} CPMAS NMR experiments used a 6.0 μs ^{1}H excitation pulse followed by a ramped CP pulse of 10 ms contact time with SPINAL-64 ^{1}H decoupling during acquisition (RF ≈41.6 kHz). ^{29}Si chemical shifts were referenced using octa(dimethylsiloxy)-octasilsesquioxane (Q8 M8H) as a secondary reference (higher frequency resonance at −2.25 ppm).

^{29}Si and ^{17}O DNP experiments: The MAS DNP experiments were carried out on a 14.1 T magnet equipped with the gyrotron operating at 395.166 GHz with 12 W power. The temperature for VT/bearing/drive gas was 92/100/105 K and 98 K without microwave irradiation. The higher drive temperature allowed us to achieve a 13 kHz spinning frequency while reducing the pressure needed. The electron paramagnetic resonance measurement was carried out prior to the MAS DNP experiments. Three freeze-thaw cycles were applied to the sample before insertion into the probe. Approximately ≈30 mg of sample was impregnated with a 16 mM solution of TEKPol in d2-tetrachloroethane (for BM_{15min}–SiO_2) or tetrabromoethane (for $Ti^*O_2+SiO_2$ and $Ti^*O_2+Si^*O_2$), leading to a toothpaste-like texture. The ^{17}O enriched phase of $TiO_2+Si^*O_2$ was impregnated with a newly developed radical which will be discussed in a future publication. The samples were then packed into a 3.2 mm thin wall zirconia rotor. The packed rotor was prespun using a benchtop spinner at room temperature to ensure stable spinning.

^{17}O{^{1}H} DNP CPMAS experiments were performed on a 3.2 mm HXY probe using HCO configuration. The initial ^{1}H CP 90° pulse was 2.5 μs, and a contact time of 50 μs with ≈100 kHz RF field. Spinal-64 ^{1}H decoupling was applied during acquisition (≈100 kHz). The spinning frequency was controlled at 13 kHz. For ^{17}O DNP DFS-echo experiments, RF was set to 100 kHz for the echo and the DFS was set to 30 kHz. Spinal-64 ^{1}H decoupling was applied during acquisition (≈100 kHz).

^{29}Si{^{1}H} DNP CPMAS experiments were performed on a 3.2 mm HXY probe using HCSi mode. The initial ^{1}H CP 90° pulse was 2.5 μs, and a contact time of 50 μs with RF of 50 kHz was used, with Spinal-64 ^{1}H decoupling during acquisition (≈100 kHz). The spinning frequency was controlled at 8 kHz.

Spectral deconvolutions and NMR parameters: All the spectral deconvolutions were performed using either DMfit[63] or Origin software. Full-width half-maximum (FWHM) is shown in ppm. Error bars were performed from 3 different fits of the experimental data, using different initial conditions, and letting parameters vary within reasonable ranges.

The quadrupolar coupling constant is noted as C_Q and shown in frequency units (Hz). The asymmetry parameter is shown as η_Q and the value is between 0 to 1. These two NMR parameters are defined using the following conventions: using V_{xx}, V_{yy}, and V_{zz} as principal components of the electric field gradient (EFG) tensor, with $|V_{yy}| \leq |V_{xx}| \leq |V_{zz}|$, then $C_Q = eQV_{zz}/h$ and $\eta_Q = (V_{yy}-V_{xx})/V_{zz}$ (with $0 \leq \eta_Q \leq 1$).[36] Moreover, the P_Q parameter was defined as $P_{Q=}C_Q\sqrt{1+\frac{\eta_Q{}^2}{3}}$.

Acknowledgements

This project has received funding from the European Research Council (ERC) under the European Union's Horizon 2020 research and innovation program (grant agreement No 772204; 2017 ERC-COG, MISOTOP project). A portion of this work was performed at the National High Magnetic Field Laboratory, which is supported by the National Science Foundation Cooperative Agreement No. DMR-1644779, the State of Florida and the United States Department of Energy. The MAS-DNP system at the NHMFL is funded in part by NIH S10 OD018519 and P41 GM122698. Financial support from the IR-RMN-THC Fr3050 CNRS for conducting part of the high-field NMR experiments is gratefully acknowledged. The UK 850 MHz solid-state NMR Facility used in this research was funded by EPSRC and BBSRC, as well as the University of Warwick including via part funding through Birmingham Science City Advanced Materials Projects 1 and 2 supported by Advantage West Midlands (AWM) and the European Regional Development Fund (ERDF). Powder X-ray diffraction, SEM and TEM characterizations were performed with the support of the local Balard Plateforme d'Analyses et de Caractérisation (PAC Balard). The CRPG Ion Probe facility (Nancy, France) where SIMS analyses were performed is acknowledged, and Nordine Bouden is thanked for his assistance in the measurements. Prof. C. Gervais (Sorbonne Université, Paris) is acknowledged for discussions on silica surface modeling. We thank Dr. Anne Alexandre in CEREGE (Aix en Provence) for IRMS measurements.

Conflict of Interest

The authors declare no conflict of interest.

Keywords: mechanochemistry · ^{17}O · silica · solid state NMR spectroscopy · surface chemistry

[1] R. K. Iler, *The Chemistry of Silica*, John Wiley & Sons, Chichester, UK, **1979**.
[2] A. Rimola, D. Costa, M. Sodupe, J.-F. Lambert, P. Ugliengo, *Chem. Rev.* **2013**, *113*, 4216–4313.
[3] G. Hartmeyer, C. Marichal, B. Lebeau, S. Rigolet, P. Caullet, J. Hernandez, *J. Phys. Chem. C* **2007**, *111*, 9066–9071.
[4] X. Xue, M. Kanzaki, *J. Phys. Chem. B* **2001**, *105*, 3422–3434.
[5] F. Tielens, C. Gervais, J. F. Lambert, F. Mauri, D. Costa, *Chem. Mater.* **2008**, *20*, 3336–3344.
[6] S. Léonardelli, L. Facchini, C. Fretigny, P. Tougne, A. P. Legrand, *J. Am. Chem. Soc.* **1992**, *114*, 6412–6418.
[7] C. C. Liu, G. E. Maciel, *J. Am. Chem. Soc.* **1996**, *118*, 5103–5119.
[8] C. S. Ewing, S. Bhavsar, G. Veser, J. J. McCarthy, J. Karl Johnson, *Langmuir* **2014**, *30*, 5133–5141.
[9] L. T. Zhuravlev, *Colloids Surf. A* **2000**, *173*, 1–38.
[10] A. P. Legrand, *The Surface Properties of Silicas*, John Wiley & Sons, New York, **1998**.
[11] G. E. Maciel, in *Silica Surfaces Charact.* (Eds.: R. K. Harris, R. L. Wasylishen), EMagRes, **2007**.
[12] G. Engelhardt, D. Michel, *High-Resolution Solid-State NMR of Silicates and Zeolites*, Wiley, **1987**.
[13] B. Grünberg, T. Emmler, E. Gedat, I. Shenderovich, G. H. Findenegg, H.-H. Limbach, G. Buntkowsky, *Chem. Eur. J.* **2004**, *10*, 5689–5696.
[14] S. E. Ashbrook, M. E. Smith, *Chem. Soc. Rev.* **2006**, *35*, 718–735.
[15] I. Farnan, P. J. Grandinetti, J. H. Baltisberger, J. F. Stebbins, U. Werner, M. A. Eastman, A. Pines, *Nature* **1992**, *358*, 31–35.
[16] T. M. Clark, P. J. Grandinetti, P. Florian, J. F. Stebbins, *Phys. Rev. B* **2004**, *70*, 64202–8.
[17] S. E. Ashbrook, Z. H. Davis, R. E. Morris, C. M. Rice, *Chem. Sci.* **2021**, *12*, 5016–5036.
[18] N. Merle, J. Trébosc, A. Baudouin, I. Del Rosal, L. Maron, K. Szeto, M. Genelot, A. Mortreux, M. Taoufik, L. Delevoye, R. M. Gauvin, *J. Am. Chem. Soc.* **2012**, *134*, 9263–9275.
[19] F. A. Perras, U. Chaudhary, I. I. Slowing, M. Pruski, *J. Phys. Chem. C* **2016**, *120*, 11535–11544.
[20] N. Merle, G. Girard, N. Popoff, A. De Mallmann, Y. Bouhoute, J. Trébosc, E. Berrier, J.-F. Paul, C. P. Nicholas, I. Del Rosal, L. Maron, R. M. Gauvin, L. Delevoye, M. Taoufik, *Inorg. Chem.* **2013**, *52*, 10119–10130.
[21] F. A. Perras, K. C. Boteju, I. I. Slowing, A. D. Sadow, M. Pruski, *Chem. Commun.* **2018**, *54*, 3472–3475.
[22] P. J. Grandinetti, J. H. Baltisberger, I. Farnan, J. F. Stebbins, U. Werner, A. Pines, *J. Phys. Chem.* **1995**, *99*, 12341–12348.
[23] F. H. Larsen, S. Rossano, I. Farnan, *J. Phys. Chem. B* **2007**, *111*, 8014–8019.
[24] A. E. Geissberger, P. J. Bray, *J. Non-Cryst. Solids* **1983**, *54*, 121–137.
[25] N. M. Trease, T. M. Clark, P. J. Grandinetti, J. F. Stebbins, S. Sen, *J. Chem. Phys.* **2017**, *146*, 184505–9.
[26] G. P. M. Bignami, D. M. Dawson, V. R. Seymour, P. S. Wheatley, R. E. Morris, S. E. Ashbrook, *J. Am. Chem. Soc.* **2017**, *139*, 5140–5148.
[27] P. J. Dirken, M. E. Smith, H. J. Whitfield, *J. Phys. Chem.* **1995**, *99*, 395–401.
[28] P. J. Dirken, S. C. Kohn, M. E. Smith, E. R. H. Van Eck, *Chem. Phys. Lett.* **1997**, *266*, 568–574.
[29] C. Gervais, F. Babonneau, M. E. Smith, *J. Phys. Chem. B* **2001**, *105*, 1971–1977.
[30] F. Babonneau, J. Maquet, *Polyhedron* **2000**, *19*, 315–322.
[31] P. N. Gunawidjaja, M. A. Holland, G. Mountjoy, D. M. Pickup, R. J. Newport, M. E. Smith, *Solid State Nucl. Magn. Reson.* **2003**, *23*, 88–106.
[32] S. L. Carnahan, B. J. Lampkin, P. Naik, M. P. Hanrahan, I. I. Slowing, B. Vanveller, G. Wu, A. J. Rossini, *J. Am. Chem. Soc.* **2019**, *141*, 441–450.
[33] C.-H. Chen, E. Gaillard, F. Mentink-Vigier, K. Chen, Z. Gan, P. Gaveau, B. Rebière, R. Berthelot, P. Florian, C. Bonhomme, M. E. Smith, T.-X. Métro, B. Alonso, D. Laurencin, *Inorg. Chem.* **2020**, *59*, 13050–13066.
[34] J. Luo, Y. Zhou, C. G. Pantano, S. H. Kim, *J. Am. Ceram. Soc.* **2018**, *101*, 5419–5427.
[35] N. Bouden, J. Villeneuve, Y. Marrocchi, E. Deloule, E. Füri, A. Gurenko, L. Piani, E. Thomassot, P. Peres, F. Fernandes, *Front. Earth Sci.* **2021**, *8*, 661169–9.
[36] R. E. Wasylishen, S. E. Ashbrook, S. Wimperis, *NMR of Quadrupolar Nuclei in Solid Materials*, Wiley, **2012**.
[37] V. Martins, J. Xu, X. Wang, K. Chen, I. Hung, Z. Gan, C. Gervais, C. Bonhomme, S. Jiang, A. Zheng, B. E. G. Lucier, Y. Huang, *J. Am. Chem. Soc.* **2020**, *142*, 14877–14889.
[38] A. Wong, A. P. Howes, J. R. Yates, A. Watts, T. Anupold, J. Past, A. Samoson, R. Dupree, M. E. Smith, *Phys. Chem. Chem. Phys.* **2011**, *13*, 12213–12224.
[39] E. G. Keeler, V. K. Michaelis, C. B. Wilson, I. Hung, X. Wang, Z. Gan, R. G. Griffin, *J. Phys. Chem. B* **2019**, *123*, 3061–3067.
[40] E. R. H. Van Eck, M. E. Smith, S. C. Kohn, *Solid State Nucl. Magn. Reson.* **1999**, *15*, 181–188.
[41] M. Xu, K. D. M. Harris, J. M. Thomas, *J. Am. Chem. Soc.* **2008**, *130*, 5880–5882.
[42] W.-C. Liao, B. Ghaffari, C. P. Gordon, J. Xu, C. Copéret, *Curr. Opin. Colloid Interface Sci.* **2018**, *33*, 63–71.
[43] F. A. Perras, K. C. Boteju, I. I. Slowing, A. D. Sadow, M. Pruski, *Chem. Commun.* **2018**, *54*, 3472–3475.
[44] M. A. Hope, D. M. Halat, P. C. M. M. Magusin, S. Paul, L. Peng, C. P. Grey, *Chem. Commun.* **2017**, *53*, 2142–2145.
[45] D. Wisser, G. Karthikeyan, A. Lund, G. Casano, H. Karoui, M. Yulikov, G. Menzildjian, A. C. Pinon, A. Purea, F. Engelke, S. R. Chaudhari, D. Kubicki, A. J. Rossini, I. B. Moroz, D. Gajan, C. Copéret, G. Jeschke, M. Lelli, L. Emsley, A. Lesage, O. Ouari, *J. Am. Chem. Soc.* **2018**, *140*, 13340–13349.
[46] F. A. Perras, T. Kobayashi, M. Pruski, *J. Am. Chem. Soc.* **2015**, *137*, 8336–8339.
[47] F. A. Perras, Z. Wang, P. Naik, I. I. Slowing, M. Pruski, *Angew. Chem. Int. Ed.* **2017**, *56*, 9165–9169; *Angew. Chem.* **2017**, *129*, 9293–9297.
[48] J. Trébosc, J. W. Wiench, S. Huh, V. S.-Y. Lin, M. Pruski, *J. Am. Chem. Soc.* **2005**, *127*, 3057–3068.
[49] E. Brunner, U. Sternberg, *Prog. Nucl. Magn. Reson. Spectrosc.* **1998**, *32*, 21–57.
[50] C. Gervais, F. Babonneau, D. Hoebbel, M. E. Smith, *Solid State Nucl. Magn. Reson.* **2000**, *17*, 2–14.
[51] J. Chen, X.-P. Wu, M. A. Hope, K. Qian, D. M. Halat, T. Liu, Y. Li, L. Shen, X. Ke, Y. Wen, J. H. Du, P. C. M. M. Magusin, S. Paul, W. Ding, X.-Q. Gong, C. P. Grey, L. Peng, *Nat. Commun.* **2019**, *10*, 5420–10.
[52] J. M. Miller, L. Jhansi Lakshmi, *J. Phys. Chem. B* **1998**, *102*, 6465–6470.
[53] I. G. Shenderovich, G. Buntkowsky, A. Schreiber, E. Gedat, S. Sharif, J. Albrecht, N. S. Golubev, G. H. Findenegg, H.-H. Limbach, *J. Phys. Chem. B* **2003**, *107*, 11924–11939.
[54] S. Brunauer, P. H. Emmett, E. Teller, *J. Am. Chem. Soc.* **1938**, *60*, 309–319.
[55] E. P. Barrett, L. G. Joyner, P. P. Halenda, *J. Am. Chem. Soc.* **1951**, *73*, 373–380.
[56] F. A. Perras, J. Viger-Gravel, K. M. N. Burgess, D. L. Bryce, *Solid State Nucl. Magn. Reson.* **2013**, *51–52*, 1–15.
[57] G. Tricot, J. Trébosc, F. Pourpoint, R. Gauvin, L. Delevoye, *Annu. Rep. NMR Spectrosc.* **2014**, *81*, 145–184.
[58] Q. Wang, J. Trébosc, Y. Li, O. Lafon, S. Xin, J. Xu, B. Hu, N. Feng, J. Amoureux, F. Deng, *J. Magn. Reson.* **2018**, *293*, 92–103.
[59] X. Lu, O. Lafon, J. Trébosc, G. Tricot, L. Delevoye, F. Méar, L. Montagne, J.-P. Amoureux, *J. Chem. Phys.* **2012**, *137*, 144201–16.
[60] H. Colaux, D. M. Dawson, S. E. Ashbrook, *Solid State Nucl. Magn. Reson.* **2017**, *84*, 89–102.
[61] H. Colaux, D. M. Dawson, S. E. Ashbrook, *J. Phys. Chem. A* **2014**, *118*, 6018–6025.
[62] G. Comellas, J. J. Lopez, A. J. Nieuwkoop, L. R. Lemkau, C. M. Rienstra, *J. Magn. Reson.* **2011**, *209*, 131–135.
[63] D. Massiot, F. Fayon, M. Capron, I. King, S. Le Calvé, B. Alonso, J.-O. Durand, B. Bujoli, Z. Gan, G. Hoatson, *Magn. Reson. Chem.* **2002**, *40*, 70–76.

Manuscript received: April 20, 2021
Accepted manuscript online: June 15, 2021
Version of record online: July 22, 2021

